Time-Resolved Fluorescence Measurements on Poly(ethylene naphthalene-2,6-dicarboxylate)

C. Spies and R. Gehrke*

Hamburger Synchrotronstrahlungslabor HASYLAB at Deutsches Elektronen-Synchrotron DESY, Notkestrasse 85, D-22603 Hamburg, Germany

Received May 31, 1996; Revised Manuscript Received January 22, 1997[⊗]

ABSTRACT: The time-resolved fluorescence behavior of poly(ethylene naphthalene-2,6-dicarboxylate) (PEN) has been investigated by synchrotron radiation. Solutions of different concentrations of PEN dissolved in 1,1,1,3,3,3-hexafluoro-2-propanol (HFIP) (10^{-4} and 10^{-2} M) have been excited at a wavelength of 340 nm, and the emission has been monitored in the wavelength range from 360 to 480 nm in 10 nm steps. The measurements have been performed at two different temperatures (288 and 298 K). Nearly all decay curves can be fitted by a sum of three exponential functions. These three exponential decay time components seem to be parameters which give the main values of a distribution of decay times. We obtained such distribution functions by assuming a simple model on the basis of excitation energy migration from monomer units (donors) to excimer sites (traps) by a Förster type mechanism. These distribution functions can be fitted by a sum of three exponential functions with reliable confidence parameters. The fits on the calculated distribution functions are in good agreement with the fits obtained from the measured data. We compared these results with data obtained on amorphous PEN films excited at the same energy. Again three exponential functions are needed to fit the measured data. The measured fluorescence decay curves can also be explained by our model.

Introduction

Time-resolved fluorescence measurements are of current interest to obtain more detailed information about the photophysics behavior of polymers containing pendant aromatic groups. It is well established that after the excitation of the aromatic system of the monomer unit excimer formation can take place. Also commonly accepted is the existence of excitation energy transfer from an excited monomer unit to an excimer site. But the kinetics of excimer formation, as well as the nature of the excimers, is discussed in a variety of different models.[1−7,25] In the case of small molecules in dilute solutions, often the kinetics model proposed by Birks[8] is applicable. It is based on intermolecular excimer formation by a diffusion controlled mechanism. This model leads to biexponential fluorescence decays. Other authors have shown that a biexponential fit could also be obtained if an appropriate distribution of decay times is realized.[9−11] This was observed, e.g., for aromatic amines dissolved in polymer films.[11]

Due to the complexity of photophysics processes in aromatic polymers, often three exponential terms are needed to fit the measured decay curves. Birks' kinetics model is too simple to explain the observed behavior, or it is simply not applicable. Examples are measurements of solid poly(1-vinylnaphthalene),[1] dilute solutions of poly(N-vinylcarbazole),[2] solids and dilute solutions of poly(1-naphthylmethyl methacrylate)[3] and poly[2-(1-naphthyl)ethyl methacrylate],[3] and dilute solutions of copolymers of 1-vinylnaphthalene and methyl acrylate.[4] Therefore, the existence of three different emitting species, i.e., one monomer and two excimers[1,2] or two distinguishable monomers and one excimer,[3,4] was proposed and different extended kinetics models in analogy to Birks' model were published.[2−4] Other authors[5,6] suggested that triple-exponential decay curves might be explained by only one monomer and one intramolecular excimer species. If one takes into account that these previously named polymers contain side chain aromatic groups and excimer formation takes place by segment rotation in the polymer chains, the rate constant of excimer formation should exhibit a time dependence of $t^{-1/2}$. But also for polymers containing main chain aromatic groups, time-resolved fluorescence studies performed by Hemker et al.[7] on solid poly(ethylene terephthalate) (PET) have shown that the fluorescence decays after excitation of the monomers have to be fitted by summing three exponential functions. They concluded that the three exponential terms are not caused by three different emitting species. They argue that according to energy migration there might be an even more complex nonexponential behavior. At lower excitation energies groundstate-stable sandwich-like dimers can be excited,[12] and Hemker et al.[7] found in this case the decay to be faster but still with three exponentials in contrast to the results of Hennecke et al. who reported a biexponential decay for this wavelength region.[13]

In the present paper we report on time-resolved fluorescence measurements performed on dilute solutions and amorphous films of poly(ethylene naphthalene-2,6-dicarboxylate) (PEN). No time-resolved measurements have been published yet, but it is known that at wavelengths where the monomer units are excited the emission spectra of PEN films are dominated by a broad structureless excimer emission band.[14,15] Quenching experiments and measurements at different concentrations of PEN solutions in mixed solvents of chloroform with different amounts of *o*-chlorophenol have shown that both intermolecular and intramolecular excimer formations are possible.[15] According to the coplanar orientation of naphthalene rings and carbonyl groups as known from crystal structure analysis,[16] intramolecular excimers are probably formed by nonadjacent chromophores and should therefore be of the same nature as intermolecular excimers.[15]

We will show that excimer formation of PEN in solution can be explained by a model of migrative excitation energy transfer from excited monomer units (donors) to excimer sites (traps). Our model calculations are similar to those introduced by Mollay et al.,[17] which

[⊗] Abstract published in *Advance ACS Abstracts,* March 1, 1997.

S0024-9297(96)00795-4 CCC: $14.00

are based on the simulation of migrative excitation trapping in polymer chains containing nonrandom aromatic groups of fixed distances. These model calculations lead to distributions of decay times. We will show that the three exponentials in the fits on our measured data can be regarded as parameters describing such a distribution of decay times. To obtain more information about the excimer formation, we also performed measurements on amorphous PEN films. Amorphous films of PEN serve as a good example to study the excitation energy transfer along the chains because there is no indication for conformational disordering on the timescale of our fluorescence experiments (i.e., $10^{-7}-10^{-9}$ s).[18,19] Therefore, excimer-forming sites are fixed in the frozen amorphous state.

Experimental Section

Sample Preparation and Characterization. PEN was synthesized as described by Buchner et al.[20] For purification purposes, the polymer was dissolved in 1,1,1,3,3,3-hexafluoro-2-propanol (HFIP) and precipitated in ethanol. The powder obtained was dried under vacuum at 40 °C for 48 h. From the synthesized material, amorphous films of about 230 μm thickness were produced by meltpressing at 295 °C in vacuo for 50 s and subsequent quenching in iced water. By wide angle X-ray scattering (WAXS) it was proved that the PEN films were completely amorphous. For further characterization, the intrinsic viscosity [η] was measured in HFIP. An apparent molecular weight $M_w = 26\,000$ g/mol was calculated by using the relationship $[\eta] = KM_w^{\alpha}$. The empirical constants $K = 5.20 \times 10^{-4}$ dL g^{-1} and $a = 0.695$ were used. These values had been determined for PET[21] and are assumed to be valid for PEN, too. From these films, solutions of about 10^{-4} and 10^{-2} M were prepared in HFIP. The concentration was calculated according to the molecular weight of the repeating monomer unit, i.e., 242 g/mol. The used HFIP was tested to show no fluorescence.

Time-resolved fluorescence measurements were performed at the synchrotron radiation laboratory HASYLAB at DESY. At the experimental station VISUV (visible and UV) the pulse structure of the positron storage ring DORIS is used for time correlated single-photon counting. Well-defined light pulses of 150 ps length (full width at half maximum, fwhm) are available at repetition rates of 2 or 5 MHz. The white beam is monochromatized by means of a double-grating monochromator (Jobin Yvon type H225), which is able to reduce the stray light contribution to 3×10^{-9}. The excitation wavelength can be varied continuously from 180 to 550 nm. The sample is mounted in a temperature-controlled quartz glass cell. The PEN films were measured in transmission geometry, and the quartz glass cell was filled with glycerol to minimize refractive effects. Fluorescence light was analyzed by a secondary monochromator (Jobin Yvon type H320), and a Phillips XP2020 photomultiplier was used for photon detection. The experiment was controlled by a PC which contains a multichannel analyzer for data acquisition and an IEEE-488 card to control the monochromators. The excitation and emission bandwidth was about 4 nm (fwhm). Acquisition time was varied from a few minutes to about 40 h to obtain sufficient counts in the maximum of each decay curve. All curves were taken with at least 30 000 up to 130 000 counts in the maximum channel. The time interval between two adjacent data points was 196 ps.

Data Evaluation. For the deconvolution of multiexponential time-resolved fluorescence data, a FORTRAN 77 routine was written. The algorithm is based on linearization and least-squares fitting of the function[22]

$$F(t) = P(t'+\delta)G(t-t',A_i,\tau_i)\,\mathrm{d}t' \qquad (1)$$

with

$$G(t) = \sum_i A_i \exp(-t/\tau_i)$$

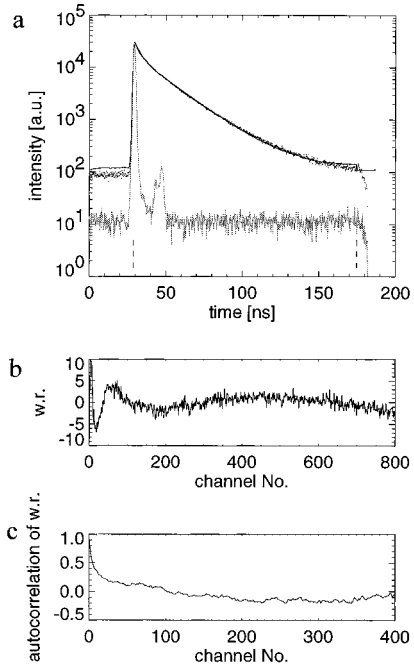

Figure 1. Example of a two-exponential fit on measured data. (a) The points (1024 channels) represent the measured fluorescence decay of PEN excited at $\lambda_{ex} = 340$ nm and emission monitored at $\lambda_{em} = 400$ nm. The solid line is the best fit obtained with a sum of two exponential functions (fit parameters: $\tau_1 = 20.30 \pm 0.03$ ns, $\tau_2 = 3.58 \pm 0.03$ ns, $A_1 = 45 \pm 0.1\%$, $A_2 = 55 \pm 0.3\%$, $\chi^2 = 3.62$, $r_m = 0.005$, and $\sigma_r = 1.9$). The dashed−dotted line shows the instrument response function. The two vertical dashed lines indicate the fitting range. (b) Weighted residuals (wr) as a function of channel number. (c) Autocorrelation.

where $P(t)$ is the measured excitation pulse shape (instrument response function), δ is a shift parameter, and $G(t)$ a sum of exponential terms with amplitudes A_i and decay times τ_i. Calculation of $F(t)$ and its first derivatives with respect to the fitting parameters is performed recursively. Routines written under IDL (Interactive Data Language) serve as an interactive user interface to the fitting routine and form a program package for data evaluation. The user interface allows for easy control over the input data, e.g., fitting range, background subtraction, initial guesses of fitting parameters, and for the convenient inspection of the results of the fitting procedure. The quality of any performed fit can immediately be examined by means of weighted residuals $r(t)$, their autocorrelation function, and confidence parameters derived from the weighted residuals, i.e., reduced χ^2, mean residuals r_m, and its standard deviation σ_r. Figures 1 and 2 show the results of a typical calculation for amorphous PEN. Figures 1a and 2a show fits with sums of two and three exponential functions, respectively. The points represent the measured data, while the solid line indicates the calculated curve. From the plots of the weighted residuals (Figures 1b and 2b) and autocorrelation function (Figures 1c and 2c), it can clearly be seen that Figure 1 represents a poor fit while the fit in Figure 2 can be accepted. The parameters of the fit and the corresponding confidence parameters are given in the figure captions. The corresponding excitation pulse (dashed−dotted lines in Figures 1a and 2a) was obtained by means of elastic scattering in milk (1.4 ns fwhm). Data were corrected to nonlinearities in the time to amplitude and analogue to digital conversion. It should also be mentioned that proper background subtraction is essential for reliable results.

Model Calculations. It could be verified that the experimental results obtained for the polymer are in good agreement with a simple model, which includes the migration of monomer excitation along a single chain, the trapping of the excitation energy at randomly distributed excimer sites, and detrapping processes. The calculation is similar to that presented by Mollay et al.[17] It is based on the evaluation of the master

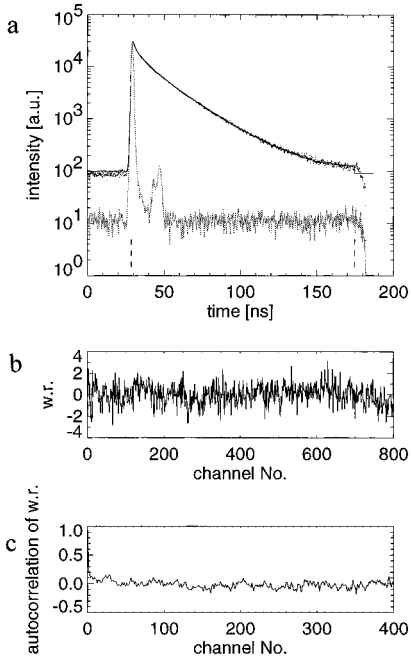

Figure 2. Example of a three-exponential fit on the data of Figure 1. (a) The points and the dashed−dotted line are the same as shown in Figure 1a). The solid line represents the best fit obtained with a sum of three exponential functions (fit parameters: $\tau_1 = 22.16 \pm 0.21$ ns, $\tau_2 = 6.99 \pm 0.11$ ns, $\tau_3 = 1.02 \pm 0.03$ ns, $A_1 = 28 \pm 0.2\%$, $A_2 = 27 \pm 0.3\%$, $A_3 = 45 \pm 1\%$, $\chi^2 = 0.91$, $r_m = 0.004$, and $\sigma_r = 0.95$). (b) Weighted reduals (wr) as a function of channel number. (c) Autocorrelation.

equation for a specific arrangement of n interacting sites:

$$\frac{d\vec{p}(t)}{dt} = \mathbf{W}\vec{p}(t) \tag{2}$$

where $\vec{p}(t) = (p_1(t), ..., p_n(t))$ is a column vector containing the probabilities $p_i(t)$ that a site i at time t is in the excited state. The sites can be monomer units (donors) or excimers (traps). $\mathbf{W} = [W_{ij}]$ is an $n \times n$ transition matrix, with elements

$$W_{ij} = (1 - \delta_{ij})\,\gamma_{ji} - \delta_{ij} \sum_{l=1, l\neq i}^{n} (\gamma_{il} + k_i) \tag{3}$$

where γ_{ij} represents the rate of energy migration from site i to j and k_i the transition rate of the radiative and nonradiative decay processes and where δ_{ij} is the Kronecker δ. If we enumerate the sites in such a way that indices $i = 1, ..., n_M$ denote the donors and $i = n_M + 1, ..., n$ denote the traps, then the solution of eq 2 can be written as

$$p_i(t) = \sum_{j=1}^{n} \left(v_{ij} \sum_{l=1}^{n} p_l(0) v_{jl}^{-1}\right) e^{\lambda_j t}, \quad i = 1, ..., n \tag{4}$$

where v_{ij} are the components of the eigenvector v_j of matrix $\mathbf{W}$ which belongs to eigenvalue λ_j (v_{ij}^{-1} are the components of inverse matrix of $[v_{ij}]$). $p_i(0)$ is the initial excitation probability of site i. If we assume that traps cannot be excited directly, we have $p_i(0) = 0$ for the traps, and if we assume that each donor site has the same probability for direct excitation, we may write $p_i(0) = 1/n_M$ for the donors. Taking this into account, we have to add all single-donor site probabilities to obtain the probability $p_M(t)$ that donors are excited at time t. One obtains

$$p_M(t) = \sum_{j=1}^{n} \left[1/n_M \sum_{i=1}^{n_M} v_{ij} \sum_{l=1}^{n_M} v_{jl}^{-1}\right] e^{\lambda_j t} = \sum_{j=1}^{n} a_{M,j} e^{\lambda_j t} \tag{5}$$

and for the corresponding excitation probability of the traps

$$p_E(t) = \sum_{j=1}^{n} \left[1/n_M \sum_{i=n_M+1}^{n} v_{ij} \sum_{l=1}^{n_M} v_{jl}^{-1}\right] e^{\lambda_j t} = \sum_{j=1}^{n} a_{E,j} e^{\lambda_j t} \tag{6}$$

Our model applies eqs 5 and 6 to a specific arrangement of donor and trap sites on a single chain described by the transition matrix $\mathbf{W}$.

For the calculation we make various assumptions: (i) Interactions causing energy transfer are effective only between adjacent sites. (ii) If i denotes a donor, the energy transfer rate γ_{ij} between two sites depends only on their distance R_{ij} and is given by isotropic dipole−dipole coupling[23]

$$\gamma_{ij} = k_M R_0^6 / |R_{ij}|^6 \tag{7}$$

where R_0 is the Förster radius and k_M is the spontaneous emission rate of the donors. This implies that we assume complete positional disorder between adjacent sites. (iii) The rate for detrapping (i.e., for γ_{ij} with i denoting a trap and j a donor) is considered to be a constant independent of the trap−donor distance. (iv) Adjacent sites are supposed to have only two distinct distances depending on whether they are in trans or gauche conformation relative to each other.

On the basis of these assumptions, N different chain configurations have been constructed by a Monte Carlo approach. Each chain configuration contains n sites, n_E of them being traps. The positions of the traps within the chain have been randomly located, as well as the distribution of trans and gauche neighborhoods, which was only determined by the probability of trans conformation. For each single configuration the set of eigenvalues $\{\lambda_j\}$ of $\mathbf{W}$ and the corresponding sets of amplitudes $\{a_{M,j}\}$ and $\{a_{E,j}\}$ were calculated using eqs 5 and 6. The amplitudes obtained from the N calculations were accumulated in m discrete channels equally spaced on a logarithmic λ scale. Finally, the mean donor and trap survival functions $\langle p_M \rangle$ and $\langle p_E \rangle$ averaged over all N configurations were calculated according to

$$\langle p_M(t) \rangle = 1/N \sum_{i=1}^{m} a_{M,(\lambda i)} e^{\lambda_i t} \tag{8}$$

and

$$\langle p_E(t) \rangle = 1/N \sum_{i=1}^{m} a_{E,(\lambda i)} e^{\lambda_i t} \tag{9}$$

Results and Discussion

First we present the results obtained from solutions of PEN in 1,1,1,3,3,3-hexafluoro-2-propanol (HFIP). HFIP is known as a good solvent with low degradation effects for PET.[21] According to the chemical similarity, it is a good solvent for PEN, too. It dissolves PEN in a wide concentration range. We have chosen two different concentrations, 10^{-2} and 10^{-4} M, to determine the influence of concentration effects on excimer formation. To obtain information about the influence of temperature on excimer formation our measurements have been performed at 288 and 298 K. Figure 3 shows emission curves of a 10^{-4} M solution of PEN in HFIP at 288 K. The sample was excited at $\lambda_{ex} = 340$ nm and the emission wavelength was varied from 360 to 470 nm in 10 nm steps. At even higher emission wavelengths, fluorescence intensity is too weak to perform reliable time-resolved measurements. All curves are normalized to the same maximum intensity. From 360 to 390 nm, the decay curves have identical shape. At higher emission wavelengths they become broader and the maximum shifts toward longer times. From this type of curve change we conclude that excimers are formed in this solution. The excimers start to emit at about 400 nm. With increasing emission wavelengths an

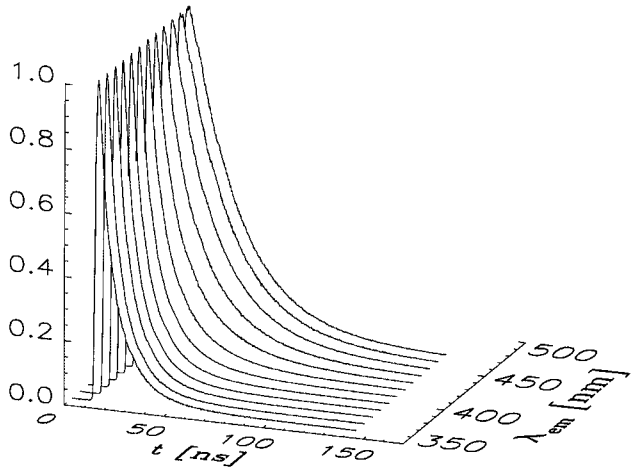

Figure 3. Fluorescence decay curves of PEN dissolved in HFIP (concentration 10^{-4} M and $T = 288$ K) excited at $\lambda_{ex} = 340$ nm as a function of time for different emission wavelengths λ_{em}. The curves are normalized to maximum intensity.

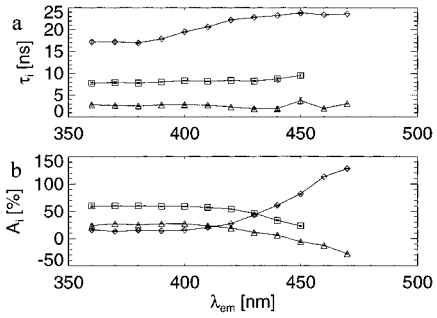

Figure 4. Parameters of the fits on measured decay curves with three or two exponential functions. (a) Calculated values of decay times $\tau_i = \lambda_i^{-1}$ of PEN dissolved in HFIP (concentration 10^{-4} M and $T = 288$ K) as a function of emission wavelength λ_{em}. (b) Corresponding amplitudes A_i (same symbols) normalized to the sum of A_i for each wavelength.

increasing amount of excimer emission is observed. It is worth mentioning here that for dimethylnaphthalene-2,6-dicarboxylate (DMN) dissolved in HFIP we also obtained the onset of the excimer emission band at 400 nm.[24] DMN can serve as a model compound of the structure unit of PEN. In order to get more information about the change of the decay curves, multiexponential fits were calculated. Figure 4 shows the obtained decay times and the corresponding amplitude values. The

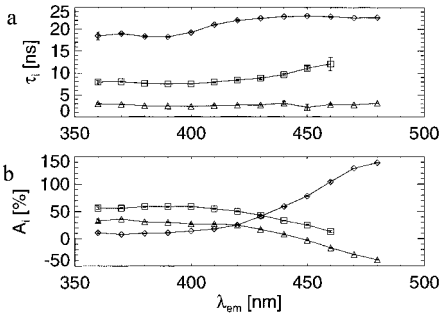

Figure 5. Parameters of the fits on measured decay curves with three or two exponential functions. (a) Calculated values of decay times $\tau_i = \lambda_i^{-1}$ of PEN dissolved in HFIP (concentration 10^{-4} M and $T = 298$ K) as a function of emission wavelength λ_{em}. (b) Corresponding amplitudes A_i (same symbols) normalized to the sum of A_i for each wavelength.

amplitudes are normalized to their sum. From 360 to 450 nm the best fits were obtained using a sum of three exponential functions. At 460 and 470 nm two exponential functions are sufficient to fit the measured data. The corresponding confidence parameters of the fits are given in Table 1. Obviously, as already mentioned for Figure 3, from 360 to 390 nm one obtains the same fit parameters within the range of error. With increasing emission wavelength the longest decay time and its amplitude increase. The amplitude of the intermediate decay time decreases, while a slight increase of the decay time itself is observed. This decay component vanishes above 450 nm. It is also worth mentioning that above 440 nm the amplitude belonging to the shortest decay time becomes negative. The observation of negative amplitudes indicates that species are emitting which were not excited directly by the incoming light pulse, i.e., at time $t = 0$. This effect is even more pronounced with increasing emission wavelength; therefore, it should be related to excimer emission.

Figure 5 shows values of decay times and corresponding amplitudes for the same sample obtained at 298 K. The measured decay curves look similar to those obtained at 298 K (see Figure 3); therefore, they are not presented. The change of the decay times as a function of emission wavelength is similar to those observed at 288 K. The amplitude values of the shortest decay time again become negative above 440 nm, but only above 460 nm only two exponentials are sufficient to obtain a good fit. Beyond this wavelength, again the intermedi-

Table 1. Confidence Parameters of the Fits at All Measured Emission Wavelengths λ_{em} ($\lambda_{ex} = 340$ nm)

	λ_{em} (nm)															
	360	370	380	390	400	410	420	430	440	450	460	470	480	490	500	510
sample a																
χ^2	0.72	0.85	0.88	1.19	1.21	1.28	0.93	0.86	1.02	1.06	0.97	0.87				
r_m	0.003	0.045	0.006	0.003	0.006	0.002	0.004	0.004	−0.003	−0.006	0.030	−0.021				
σ_r	0.85	0.92	0.94	1.08	1.09	1.13	0.96	0.92	1.00	1.02	0.98	0.93				
sample b																
χ^2	0.88	1.05	1.09	1.08	0.98	0.96	0.81	0.87	1.24	1.02	0.96	1.23	1.05			
r_m	0.037	0.044	0.031	0.008	0.044	0.041	0.034	0.020	−0.004	−0.011	−0.010	0.053	0.007			
σ_r	0.93	1.02	1.04	1.03	0.98	0.98	0.89	0.93	1.11	1.00	0.98	1.10	1.02			
sample c																
χ^2		0.74	0.80	1.12	1.20	1.61	1.24	0.90	0.98	0.93	1.01	1.36	0.92			
r_m		0.038	0.034	0.013	−0.006	−0.008	0.008	−0.001	0.009	−0.005	−0.015	−0.07	−0.05			
σ_r		0.86	0.89	1.05	1.09	1.26	1.11	0.94	0.99	0.96	1.00	1.16	0.96			
sample d																
χ^2				0.92	0.91	0.83	0.98	0.83	0.96	0.72	0.79	0.85	0.85	0.82	0.78	0.86
r_m				0.098	0.005	0.026	0.009	−0.003	0.001	0.002	0.017	0.001	−0.005	0.005	0.004	0.008
σ_r				0.95	0.95	0.91	0.99	0.91	0.98	0.84	0.88	0.92	0.92	0.90	0.88	0.93

[a] Sample a: PEN dissolved in HFIP, concentration 10^{-4} M and $T = 288$ K. [b] Sample b: PEN dissolved in HFIP, concentration 10^{-4} M and $T = 298$ K. [c] Sample c: PEN dissolved in HFIP, concentration 10^{-2} M and $T = 298$ K. [d] Sample d: Amorphous PEN film.

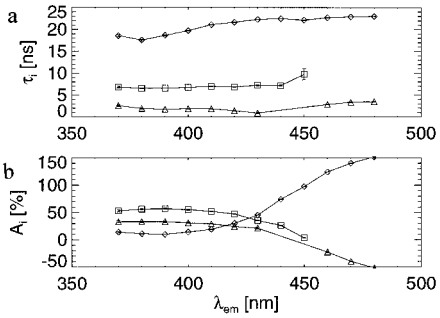

Figure 6. Parameters of the fits on measured decay curves with three or two exponential functions. (a) Calculated values of decay times $\tau_i = \lambda_i^{-1}$ of PEN dissolved in HFIP (concentration 10^{-2} M and T = 298 K) as a function of emission wavelength λ_{em}. (b) Corresponding amplitudes A_i (same symbols) normalized to the sum of A_i for each wavelength.

ate decay time vanishes. The change of the amplitude values as a function of emission wavelength is also similar to the data obtained at 288 K. However, in comparison with Figure 4, the mean values of the amplitudes obtained for the range from 360 to 390 nm are slightly different. The values obtained for the shortest and the intermediate decay time are basically identical to those obtained at 288 K, while the longest decay time is slightly increased. The calculated mean values from 360 to 390 nm will be mentioned later.

Figure 6 shows observed decay times and corresponding amplitudes of a 10^{-2} M solution of PEN in HFIP measured at 298 K. The solution was again excited at $\lambda_{ex} = 340$ nm, and the emission wavelength was varied from 370 to 480 nm. Only slight changes are observed by increasing the concentration of 2 orders of magnitude. For this higher concentrated solution in the range of $\lambda_{em} = 370-390$ nm the average values of the shortest and the intermediate decay time are slightly shorter than the corresponding values obtained on a 10^{-4} M solution. All other values only vary within the range of error. Compared with those of the 10^{-4} M solution, the changing of the decay times and amplitudes of the 10^{-2} M solution as a function of emission wavelength is similar. Differences are only observed at 440 and 450 nm where the best fit is obtained with a sum of two exponential function. In contrast to previously obtained results, the shortest decay time vanishes. Above 450 nm the shortest decay time appears again, while the intermediate decay time vanishes.

In order to interpret our results, a model of two polymer chains is given in Figure 7. On the left hand side the monomer unit of PEN is shown. We assume that the aromatic systems of the monomer units are excited randomly by the excitation pulse. The formation of excimers is possible at locations where the polymer chains form loops or where neighboring chains are situated close to each other. In accordance with Renamayor et al.,[25] we suppose that excimers are only formed by interaction of an excited monomer unit with another monomer unit in the electronic ground state. To obtain a strong interaction of the π-orbitals, excimers are probably sandwich-like formations of aromatic ring pairs. The corresponding picture is outlined on the right hand side of Figure 7. The sandwich-like formation drawn in this figure is intended only to serve as a model. We cannot say anything about the exact geometry of an excimer. If monomer units in the polymer chains are excited, the excitation energy can migrate along the chain. This migration mechanism could be explained by a Förster type dipole−dipole interaction.[23] When a

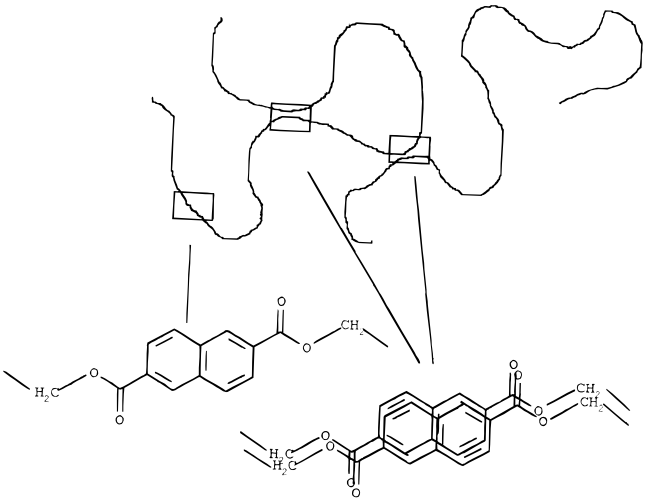

Figure 7. Model of excimer forming sites in a polymer containing aromatic groups in the main chain, e.g., PEN. Left hand side: Monomer unit of PEN. Right hand side: Schematically drawn model of an excimer.

suitable conformation of two neighboring chains or of an intramolecular loop is reached, the excitation is trapped by the formation of an excimer. Time-resolved fluorescence depolarization experiments on amorphous PEN films have shown that excitation energy transfer takes place on a picosecond time scale after the excitation of a monomer site.[26]

We describe in another paper the time-resolved fluorescence behavior of dimethylnaphthalene-2,6-dicarboxylate (DMN).[24] DMN serves as a model compound of the structural unit of PEN. For dilute solutions of 10^{-4} M DMN in HFIP, we observed monoexponential decays over the whole emitting range. The monoexponential decays of DMN in very dilute solutions of HFIP directly resemble the lifetime τ of the monomers. The lifetime of DMN in HFIP is 12.72 ns measured at 288 K and gives a monomer decay rate constant $k_M = k_{FM} + k_{IM} = 7.86 \times 10^7$ s^{-1}. For higher concentrations of DMN, e.g., 10^{-1} M, excimer formation is observed. In this case Birks' kinetics model can be applied. Excimers are formed with rate k_{EM}, dissociate with rate k_{ME}, and perform radiative and nonradiative decay transitions with rate k_E. Experimentally, one obtains the decay times $\tau_i = \lambda_i^{-1}$ and corresponding amplitudes of these biexponential decays. To estimate the rate constants, we considered additional boundary conditions. The sum of the reciprocal decay times is equal to the sum of all rate constants. From the energy range where only monomers emit the values of amplitudes for the decay of monomers is known. The rate constant of pure monomer emission was obtained from dilute solutions, i.e., 10^{-4} M. With $k_M = 7.86 \times 10^7$ s^{-1}, $k_{EM}[M] = 6.0 \times 10^7$ s^{-1}, $k_{ME} = 1.16 \times 10^7$ s^{-1}, and $k_E = 4.1 \times 10^7$ s^{-1} we find an excellent agreement between the theoretically calculated and experimentally obtained values for the monomer fluorescence for a 10^{-1} M solution at 288 K.[24]

The PEN calculations were performed on the basis of the model described in the Experimental Section. From geometrical considerations based on data reported by Mencik,[16] one can estimate a mean R_{trans} of 1.37 nm for the distance of two adjacent chromophores in trans conformation relative to each other, while the distance for a gauche conformation is about 1.06 nm. Assuming a Förster radius of 3.5 nm and a donor decay rate $k_M = 7.86 \times 10^7$ s^{-1}, we find with eq 7 values of 2.1×10^{10}

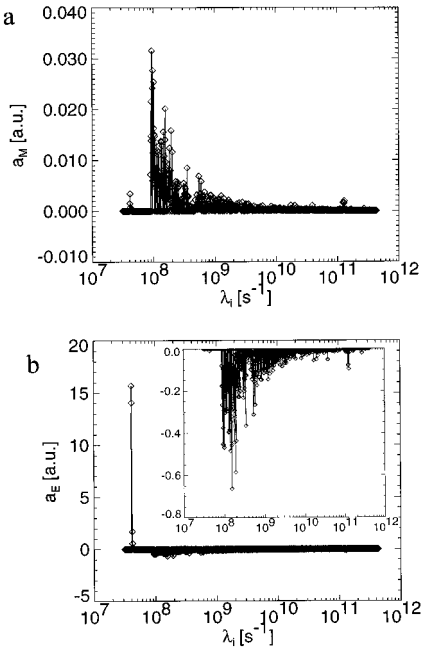

Figure 8. Results of model calculations performed for PEN dissolved in HFIP (concentration 10^{-4} M and T = 288 K). (a) Amplitude distribution versus donor reciprocal decay times λ_i. (b) Amplitude distribution versus trap reciprocal decay times. Insertion: Magnified representation of negative amplitude values.

s^{-1} and 1.0×10^{11} s^{-1} for the energy migration rates between neighbors in trans and gauche conformation, respectively. The donor decay rate was obtained from the measurements of dilute solutions of DMN in HFIP. For the trap decay and trap dissociation rates, we used the values previously calculated for DMN in concentrated HFIP solutions,[24] i.e., $k_E = 4.1 \times 10^7$ s^{-1} and $k_{ME} = 1.16 \times 10^7$ s^{-1}. We suggest that this trap dissociation rate is a good estimation for PEN solutions because the trap dissociation is assumed to be mainly influenced by solvent interactions. The solvent interactions should be similar in both cases. We performed the model calculations on the basis of 100 sites within the chain in accordance to the estimated molecular weight of our sample. Two sites were regarded as excimer traps. Finally, as revealed by ^{2}H-NMR data[18] for the randomly coiled amorphous regions, about 50% of the sites were assumed to be in trans conformation to each other. On the basis of these assumptions, the results were obtained by averaging over 100 chain samples. From the calculations, we find distributions of amplitudes $a_M(\lambda)$ for the monomers (donors) and $a_E(\lambda)$ for the excimers (traps) as shown in Figure 8. For the monomer emission all amplitudes have positive values. Values for λ_i are located around 4×10^7 s^{-1} and an additional broad distribution is ranging from 1×10^8 s^{-1} to about 1×10^{11} s^{-1}. For the excimer emission only the amplitude values located around 4×10^7 s^{-1} are positive while all others are negative. The corresponding decay curves $p_M(t)$ for the donors and $p_E(t)$ for the traps are given in Figure 9. A fast donor decay is observed. The decay of the traps is comparatively slow and its maximum is shifted toward longer times. Note that our monomer curve has been multiplied by a factor of 20 to obtain comparable magnitudes in the plot. Note also that the functions $p_M(t)$ and $p_E(t)$ only give the probabilities at a given time t after the excitation pulse monomers and excimers are in an excited state. In order to obtain the ratio of monomer and excimer emission intensity at a given wavelength, these functions would have to be

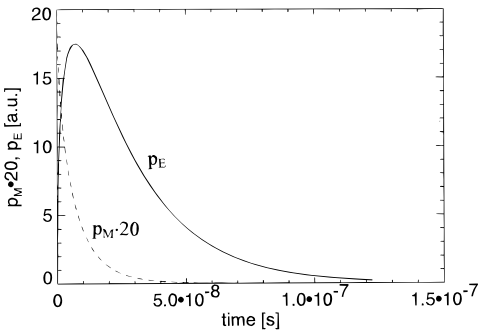

Figure 9. Calculated decay curves obtained from the distribution functions of Figure 8. The solid line represents the excimer (trap) decay curve. The dashed line shows the monomer (donor) decay curve multiplied by a factor of 20.

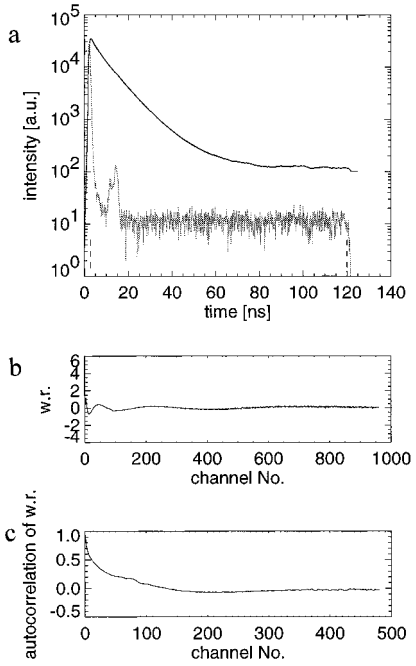

Figure 10. Three-exponential fit on the calculated donor decay curve of Figure 9. (a) Solid lines show the calculated and fitted curves (fit parameters: $\tau_1 = 13.59 \pm 0.38$ ns, $\tau_2 = 7.47 \pm 0.14$ ns, $\tau_3 = 2.07 \pm 0.09$ ns, $A_1 = 12 \pm 1\%$, $A_2 = 62 \pm 1\%$, $A_3 = 26 \pm 1\%$, $\chi^2 = 0.03$, and $r_m = 0.03$). Dashed−dotted line: Instrument response function which was convoluted with the model data before fitting. (b) Weighted residuals (wr) as a function of channel number. (c) Autocorrelation.

multiplied with the spectral functions of the excimer and monomer emission, respectively.

By fitting the monomer (donor) decay curve from this model calculations with the same procedure which we applied to the measured data, i.e., by summing three exponential functions, we obtain the results shown in Figure 10. Prior to this fitting, the donor decay curve of Figure 9 was convoluted with a measured instrument response function. We only chose the donor decay curve because, according to weak intensity, we could not measure pure trap emission with sufficiently reliable statistics to compare them with the calculated curve. The calculated parameters are $\tau_1 = 13.59 \pm 0.38$ ns, $\tau_2 = 7.47 \pm 0.14$ ns, $\tau_3 = 2.07 \pm 0.09$ ns, $A_1 = 12 \pm 1\%$, $A_2 = 62 \pm 1\%$, and $A_3 = 26 \pm 1\%$ ($\chi^2 = 0.03$ and $r_m = 0.03$). The experimental results for PEN dissolved in HFIP at 288 K and excited at 340 nm are $\tau_1 = 17.28 \pm 0.34$ ns, $\tau_2 = 7.90 \pm 0.10$ ns, $\tau_3 = 2.69 \pm 0.11$ ns, $A_1 = 14 \pm 1\%$, $A_2 = 60 \pm 1\%$, and $A_3 = 26 \pm 1\%$. These are the mean values calculated from the emission range of pure monomer emission, i.e., 360−390 nm. Although the

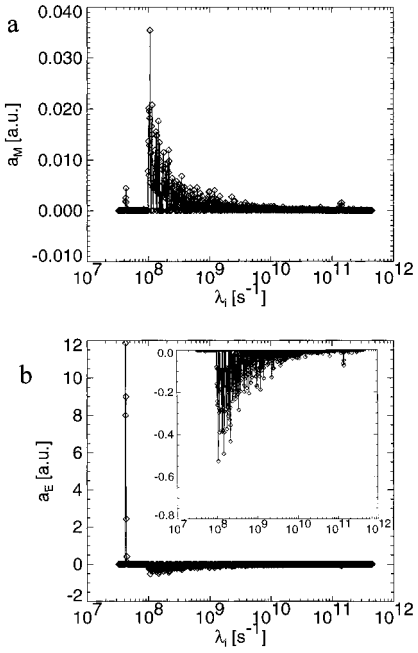

Figure 11. Results of model calculations performed for PEN dissolved in HFIP (concentration 10^{-4} M and $T = 298$ K). (a) Amplitude distribution versus donor reciprocal decay times λ_i. (b) Amplitude distribution versus trap reciprocal decay times. Insertion: Magnified representation of negative amplitude values.

model calculations include some rather simplifying assumptions, we get a reasonable agreement between measured and calculated data. Taking into account that for most emission wavelengths emission of donors and traps is monitored simultaneously, the change from triple- to biexponential decay curves at higher emission wavelength as shown in Figure 4 can be explained with these distribution functions. The magnitude of a_E/a_M obtained from Figure 8 increases continuously in the range from $\lambda_i = 10^8$ to 10^9 s^{-1}. Thus compositions of excimer and monomer intensities exist where the intermediate decay vanishes and only the shortest appears with negative values. Also, the increase of the amplitude value of the longest decay time with an increasing amount of excimer emission intensity can be explained. The distribution function of pure excimer emission a_E shows large positive amplitude values located around $\lambda_i = 4 \times 10^7$ s^{-1} which leads to a decay time $\tau_i = \lambda_i^{-1}$ of about 25 ns. Therefore, with an increasing amount of excimer emission intensity, the amplitude value of the longest decay had to increase. This demonstrates that these model calculations also describe the change of the measured decay curves as a function of emission wavelength.

For our measurements carried out at 298 K we performed calculations with rate constants obtained for DMN in HFIP at this higher temperature.[24] For the trap decay rate and for trap dissociation, we calculated the values $k_E = 4.2 \times 10^7$ s^{-1} and $k_{ME} = 2.1 \times 10^7$ s^{-1}.[24] Again, assuming a Förster radius of 3.5 nm with $k_M = 8.70 \times 10^7$ s^{-1} ($\tau_m = 11.49$ ns) and eq 7, we find for the energy migration rate between neighbors in trans and gauche conformation 2.42×10^{10} s^{-1} and 1.1×10^{11} s^{-1}, respectively. Again, we assumed a 100 segment chain with 50% trans configuration of adjacent ethylene groups and performed an average over 100 calculations. Figure 11 shows the distributions of amplitudes for donor and trap excitation. The obtained distributions look similar to those calculated with the values measured at 288 K. Therefore, the corresponding decay curves $p_M(t)$ and $p_E(t)$ are not represented. We got the best triple-exponential fit on the calculated monomer decay curve $p_M(t)$ with $\tau_1 = 17.02 \pm 0.44$ ns, $\tau_2 = 7.35 \pm 0.08$ ns, $\tau_3 = 2.12 \pm 0.06$ ns, $A_1 = 5 \pm 1\%$, $A_2 = 63 \pm 1\%$, and $A_3 = 32 \pm 1\%$ ($\chi^2 = 0.06$ and $r_m = 0.03$). From the fits on the measured curves, again we calculated the mean values of the emission range 360−390 nm. These mean values are $\tau_1 = 18.49 \pm 0.28$ ns, $\tau_2 = 7.76 \pm 0.22$ ns, and $\tau_3 = 2.70 \pm 0.22$ ns; the corresponding amplitudes are $A_1 = 10 \pm 1$, $A_2 = 58 \pm 2$, and $A_3 = 32 \pm 2$. The fits obtained on the calculated distribution function and on the measured data are in good agreement. Compared with the values obtained on the measured curves at 288 K, τ_2 and τ_3 are identical within the range of error while τ_1 increases. We obtained a decrease of A_1 and an increase of A_3 while A_2 stays constant. This observation is also revealed for the fits on the calculated distribution functions.

In order to interpret the effect of temperature on excimer formation, we compared these results again with the excimer formation obtained for DMN in HFIP in 10^{-1} M solution. We found that all four rate constants of the Birks' scheme are temperature dependent.[24] Our calculations for the polymer chain took care of the temperature influence of monomer emission, excimer emission, and excimer dissociation. And we got good agreement between measured and calculated curves. Our model calculations for the excimer formation in the polymer are not influenced by a diffusion controlled mechanism. The diffusion-controlled rate constants of excimer formation $k_{ME}[M]$ for the small molecule DMN in HFIP were presented in another paper.[24] For a 10^{-1} M solution the values $k_{ME}[M] = 6.0 \times 10^7$ s^{-1} at 288 K and 7.58×10^7 s^{-1} at 298 K were calculated.[24] The rate of the diffusion process of small molecules is much slower than the rates of observed energy migration in a polymer chain. Taken into account that a diffusion of monomer units fixed in a polymer chain should be even slower, the main process of excimer formation is excitation energy migration. Therefore, we conclude that, for example, a loop has to be formed and then by the migrative mechanism the excimer is built.

To explain the results obtained on 10^{-2} M solution, we first want to point out that an increase of the concentration of 2 orders of magnitude has a very slight effect on the time resolved fluorescence behavior. The first observation is that the mean values calculated in the range from 370 to 390 nm, i.e., pure monomer emission, are nearly the same. The calculated average values from the fits on the measured curves are $\tau_1 = 18.25 \pm 0.50$ ns, $\tau_2 = 6.63 \pm 0.13$ ns, $\tau_3 = 2.08 \pm 0.37$ ns, $A_1 = 12 \pm 2$, $A_2 = 55 \pm 2$, and $A_3 = 33 \pm 1$. Except τ_2 and τ_3, which are found to be slightly shorter, all other values only vary within the range of error. The next point is the similarity of the changing of τ_i's and A_i's as a function of emission wavelength compared with the results obtained on the 10^{-4} M solution. The only difference was observed at 440 and 450 nm where biexponential decays occur with the shortest decay time disappearing. Our first approach was to increase the number of traps assuming that a higher concentration increases the number of trap sites. But an increase from two to three traps per chain does not lead to a better agreement between the fits of the measured and calculated curves. Considering that each chain solved in a 10^{-4} M solution forms an isolated coil, there might

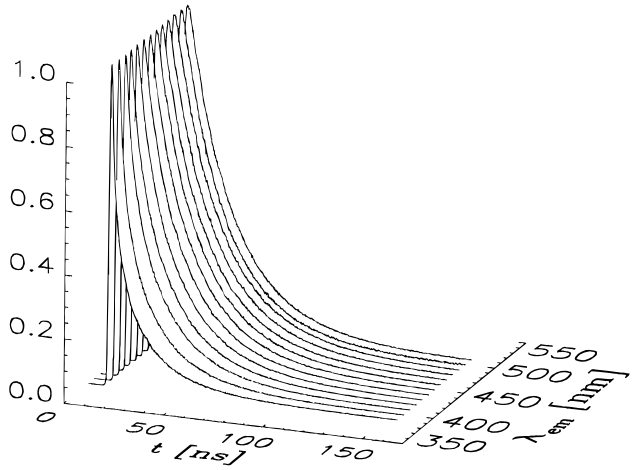

Figure 12. Fluorescence decay curves of an amorphous PEN film excited at $\lambda_{ex} = 340$ nm as a function of time for different emission wavelengths λ_{em}. The curves are normalized to maximum intensity.

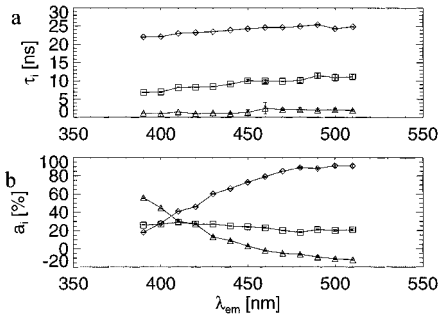

Figure 13. Parameters of the fits on measured decay curves with three exponential functions. (a) Calculated values of decay times $\tau_i = \lambda_i^{-1}$ of an amorphous PEN film as a function of emission wavelength λ_{em}. (b) Corresponding amplitudes A_i (same symbols) normalized to the sum of A_i for each wavelength.

be no interaction between different chains. In solutions of higher concentrations the coils might still have the same shape, and this means that there would be no evidence for an increasing number of intramolecular formed traps. When the concentration is increased, the coils might only come closer to each other. They might not be close enough to form intermolecular excimers, but excitation energy transfer to neighboring chains might be already possible. We cannot address this situation with our model because it involves a continuous range of distances over which this transfer takes place. However, in this case the dominant transfer mechanism would be still the same as before and only a few transfers would have different rates. Thus one would expect only a minor change of distribution function as we observed by our measurements.

The next point to discuss is the assumption of our model calculations that only one type of excimer is formed. According to Verbeek et al.,[11] an emitting species is influenced by its surrounding and this also leads to a distribution of decay times. However, in the case of dilute solutions we assume that there should be an optimal excimer configuration exhibiting a minimum potential energy. The main point is that solutions of the small molecule DMN show biexponential decays[24] while the polymer gives triple exponential decays. If there is a distribution of different types of excimers according to different groupings i.e., a grouping where only parts of the rings can overlap, or different distances this should be observed in both cases. If there exists such an overlaid distribution of decay times, it has only a minor effect for the explanation of our observed fluorescence decay curves. Therefore, we conclude that an optimal configuration of excimer formation is a good assumption and the main point of obtaining a distribution of lifetimes in a solution of an aromatic main chain polymer is the excitation energy migration.

Next we will present the results obtained on a solid amorphous PEN film. It was also excited at wavelength $\lambda_{ex} = 340$ nm and the emission wavelength λ_{em} was varied from 390 to 510 nm in 10 mm steps. Figure 12 shows the fluorescence intensity as a function of time for different emission wavelengths. Measurements were carried out at room temperature. With increasing emission wavelength, one observes broader decay curves and a slight shift of the maximum toward larger times. This observation is comparable with the measurement of PEN dissolved in HFIP (see Figure 3). Thus, we assume that this change can be explained again by an increasing amount of excimer emission intensity with increasing emission wavelength. However, in the solid amorphous state, the fluorescence decay curves are narrower than in dilute solutions and the shift of the maximum is smaller. This effect is even more pronounced in Figure 13. Figure 13 represents the fit parameters on the measured decay curves. To obtain good agreement between measured and calculated curves, three exponential function are required for the fitting. At 390 nm, the shortest decay time has a value of about 1.1 ns and an amplitude value A_3 of about 56%. As a function of emission wavelength, the amplitude value A_3 decreases and negative values occur above 450 nm. The amplitude value of the longest decay time increases, and only a slight decrease of the amplitude belonging to the intermediate decay time is observed. We want to point out that for 500 and 510 nm we obtained identical parameters within the range of error. Therefore, we conclude that pure excimer emission is reached in this range. The main difference to the results mentioned previously for solutions is the observation of two positive and only one negative amplitude value in the region of pure excimer emission. On the other hand, we are not sure that we monitored pure monomer emission at 390 nm. As known from the literature, in other solvents the onset of an excimer emission band was observed in this emission range.[15] Thus, in the solid state we do not know were the excimer starts to emit; however, at 390 nm the fluorescence decay curve is dominated by monomer emission.

For the amorphous polymer, calculations were performed using the same model as before. Again, a Förster radius of 3.5 nm and the same value for the excimer emission rate $k_E = 4.2 \times 10^7\ s^{-1}$ was assumed. To obtain excimer distributions with two distinct mean amplitudes with positive sign and a short negative one, we had to increase the number of traps. Next, we had to assume a faster excimer back reaction (k_{EM}) and we also had to increase the value of donor decay rate k_M. With the values $k_{EM} = 1 \times 10^9\ s^{-1}$, $k_M = 3 \times 10^8\ s^{-1}$, and five traps we calculated the distribution functions represented in Figure 14. By means of eq 7, we used this donor rate to calculate the energy migration rate for neighbors in trans and gauche conformation to be $8.35 \times 10^{10}\ s^{-1}$ and $3.89 \times 10^{11}\ s^{-1}$, respectively. For pure monomer emission shown in Figure 14a, the largest values of amplitudes are located around $10^9\ s^{-1}$, which is in good agreement with the values of the fit on our measured data at 390 nm. Pure excimer emis-

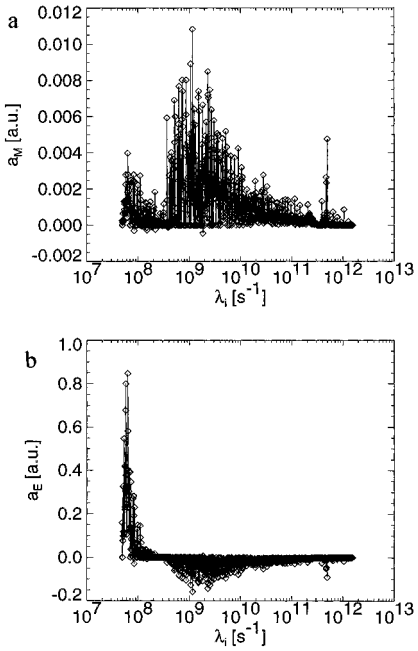

Figure 14. Results of model calculations performed for amorphous PEN films. (a) Amplitude distribution versus donor reciprocal decay times λ_i. (b) Amplitude distribution versus trap reciprocal decay times.

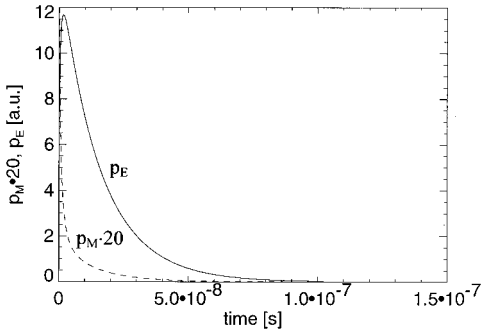

Figure 15. Calculated decay curves obtained from the distribution functions of Figure 14. The solid line represents the excimer (trap) decay curve. The dashed line shows the monomer (donor) decay curve multiplied by a factor of 20.

sion as shown in Figure 14b leads to a broad distribution of positive amplitudes in the range from 5×10^7 s^{-1} to 2×10^8 s^{-1} and negative values of amplitudes around 1×10^9 s^{-1}. Figure 15 represents the decay curves $p_M(t)$ and $p_E(t)$ obtained from the distribution functions for pure monomer and pure excimer emission, respectively. Compared with the results obtained on the solutions of Figure 9, the monomer decay is narrower and the excimer decay shows a smaller shift of the maximum as observed in the measured fluorescence decay curves. The different rate constants for the back-reaction from excimer to monomer excitation found for solutions and solid samples can be explained at least qualitatively if one accounts for the different physical mechanisms involved. In solutions, the rate of back-reaction processes might be given by the probability of a collision between the excimer site and another molecule carrying sufficient kinetic energy. The latter will be most probably a solvent molecule. In the solid, the back-reaction rate is proportional to the local density of phonons with energies beyond the energy necessary to initiate the dissociation of the excimer. To obtain more information about the values of the rate constants, further investigations are necessary. However, we have shown that our model of excimer formation is also applicable for the solid amorphous state.

Conclusions

The fluorescence behavior of PEN dissolved in HFIP, as well as in the solid amorphous state, can be described by assuming a simple model of only one type of emitting monomer and one type of emitting excimer. To fit the fluorescence decay curves observed by the experiments, nearly in all cases three exponential functions are necessary. We have shown that these three exponential functions can be taken as parameters which give the main values of a distribution of decay times. This distribution of decay times is caused by the mechanism of excimer formation and dissociation. Excimers are formed by excitation energy transfer from monomer unit to monomer unit along the polymer chain until it arrives at a suitable conformation. Excimers are assumed to be sandwich-like formations of two aromatic rings. Therefore, these conformations should be realized where a polymer chain forms loops (intramolecular) or by two neighboring chains situated close to each other (intermolecular) and their emission should be indistinguishable. Nevertheless, the number of excimer forming sites has a strong effect of the calculated distribution functions. The probability of the formation of intramolecular excimers in solutions is in connection to the chain length (molecular weight) and the used solvent, i.e., the coil dimension is influenced by the nature of the solvent at a given temperature. The probability of intermolecular excimer formation of neighboring chains is mainly influenced by the concentration of the solution. Our calculations consider the chain length of the polymer. From the results obtained with our PEN sample (M_w = 26 000 g/mol, i.e., about 100 monomer sites) in dilute solutions of HFIP, i.e., 10^{-4} M, we conclude that isolated coiled chains with two traps are formed. An increase of the concentration of two orders of magnitude leads to the results that the coils are still not close enough for intermolecular excimer formation. In contrast to polymer solutions, the results obtained from the small molecule DMN dissolved in HFIP show that an increase of the concentration from 10^{-4} M to 10^{-2} M leads to a change from monoexponential to biexponential fluorescence decays, i.e., a diffusion controlled mechanism for excimer formation was observed.[24] This leads to the conclusion that the process of excimer formation in such an aromatic main chain polymer is not diffusion controlled, because diffusion is much slower than excitation energy transfer. Decreasing the temperature from 298 to 288 K has no effect on the number of excimer forming sites per chain. A slight change of the fluorescence decay curves, revealed in a slight change of the decay parameters obtained by the fits on the measured curves, can be explained by the temperature dependence of the rate constants of pure monomer emission, pure excimer emission, and excimer dissociation. To explain the fluorescence decay curves obtained from a solid amorphous PEN film, the number of traps in the model has to be increased. We assumed a number of five traps per chain, and additionally, the rate of pure monomer emission and excimer dissociation had to be increased. In the case of the solid state we conclude that the back-reaction rate is proportional to the local density of phonons with energies beyond the energy necessary to initiate the dissociation. In the frozen amorphous state there might exist a distribution of excimer-forming sites. However, we assume that the effect of excimer formation by excitation energy transfer is much more pro-

nounced in the observed fluorescence decay curves. Therefore, we conclude that the presented simple model is also a good approximation for the solid amorphous state. Finally, we conclude that the presented model should be applicable for all such types of polymers containing aromatic main chain groups. The main requirements are a distance between two aromatic systems much closer than the Förster radius and a separation of these aromatic systems by groups which prevent delocalization of the π-orbitals of neighboring aromatic rings.

Acknowledgment. We thank Professor Zachmann for giving us the opportunity of sample preparation in his laboratory. This work was granted by a post doctoral fellowship of the Arbeitsgemeinschaft Grossforschung AGF.

References and Notes

(1) Coulter, D. R.; Liang, R. H.; DiStefano, S.; Moacanin, J.; Gupta, A. *Chem. Phys. Lett.* **1982**, *87*, 594.
(2) Ng, D.; Guillet, J. E. *Macromolecules* **1981**, *14*, 405.
(3) Holden, D. A.; Wang, P. Y.-K.; Guillet, J. E. *Macromolecules* **1980**, *13*, 295.
(4) Phillips, D.; Roberts, A. J.; Soutar, I. *Polymer* **1981**, *22*, 293.
(5) Itagaki, H.; Kazuyuki, H.; Mita, I. *Macromolecules* **1983**, *16*, 1395.
(6) Fredrickson, G. H.; Frank, C. W. *Macromolecules* **1983**, *16*, 572.
(7) Hemker, D. J.; Curtis, W. F.; Thomes, J. W. *Polymer* **1988**, *29*, 437.
(8) Birks, J. B. *Photophysics of Aromatic Molecules*; Wiley-Interscience: New York, 1970.
(9) James, D. R.; Ware, W. R. *Chem. Phys. Lett.* **1985**, *120*, 455.
(10) James, D. R.; Ware, W. R. *Chem. Phys. Lett.* **1986**, *126*, 7.
(11) Verbeek, G.; Vaes, A.; Van der Auweraer, M.; DeSchryver, F. C.; Geelen, C.; Terrell, D.; De Meutter, S. *Macromolecules* **1993**, *26*, 472.
(12) Hennecke, M.; Fuhrmann, J. *Makromol. Chem., Macromol. Symp.* **1986**, *5*, 181.
(13) Hennecke, M.; Kud, A.; Kurz, K.; Fuhrmann, J. *Colloid Polym. Sci.* **1987**, *265*, 674.
(14) Phillips, D. H.; Schug, J. C. *J. Chem. Phys.* **1969**, *50*, 3297.
(15) Shangxian, C.; Fenglian, B.; Renyuan, Q. *Sci. Sin. (Engl. Ed.)* **1981**, *24*, 639.
(16) Mencik, Z. *Chem. Prum.* **1967**, *17*, 78.
(17) Mollay, B.; Kauffmann, H. F. *Macromolecules* **1994**, *27*, 5129.
(18) Dörlitz, H.; Zachmann, H. G. *J. Macromol. Sci., Phys.* Submitted for publication.
(19) Ezquerra, T. A.; Balta-Calleja, F. J.; Zachmann, H. G. *Acta Polym.* **1993**, *44*, 18.
(20) Buchner, S.; Wiswe, D.; Zachmann, H. G. *Polymer* **1989**, *30*, 480.
(21) Berkowitz, S. *J. Appl. Polym. Sci.* **1984**, *29*, 4353.
(22) Bevington, P. B. *Data Reduction and Error Analysis for the Physical Science*; McGraw-Hill, New York, 1969.
(23) Agranovich, V. M.; Galanin, M. D. *Electronic Excitation Energy Transfer in Condensed Matter*; North Holland, New York, 1982.
(24) Spies, C.; Gehrke, R. To be published.
(25) Renamayor, C. S.; Gomez-Anton, M. R.; Calafate, B.; Mano, E. B.; Radic, D.; Gargallo, L.; Freire, J. J.; Pierola, I. F. *Macromolecules* **1991**, *24*, 3328.
(26) Spies, C.; Gehrke, R. Internal HASYLAB annual report. Part II. HASYLAB: Hamburg, 1995; p 87.

MA960795N